HHS Public Access

Author manuscript

Cell Rep. Author manuscript; available in PMC 2016 July 21.

Published in final edited form as:

Cell Rep. 2016 July 19; 16(3): 793–804. doi:10.1016/j.celrep.2016.06.032.

Impaired Recall of Positional Memory following Chemogenetic Disruption of Place Field Stability

Rong Zhao[1,9], **Stacy D. Grunke**[1,9], **Madhusudhanan M. Keralapurath**[1], **Michael J. Yetman**[1], **Alexander Lam**[1,6], **Tang-Cheng Lee**[1], **Konstantinos Sousounis**[1], **Yongying Jiang**[7], **Deborah A. Swing**[8], **Lino Tessarollo**[8], **Daoyun Ji**[1,2,*], and **Joanna L. Jankowsky**[1,3,4,5,*]

[1]Department of Neuroscience, Baylor College of Medicine, Houston, TX 77030, USA

[2]Department of Molecular and Cellular Biology, Baylor College of Medicine, Houston, TX 77030, USA

[3]Department of Neurology, Baylor College of Medicine, Houston, TX 77030, USA

[4]Department of Neurosurgery, Baylor College of Medicine, Houston, TX 77030, USA

[5]Huffington Center on Aging, Baylor College of Medicine, Houston, TX 77030, USA

[6]Department of Cognitive Science, Rice University, Houston, TX 77251, USA

[7]Institute for Applied Cancer Science, The University of Texas MD Anderson Cancer Center, Houston, TX 77054, USA

[8]Mouse Cancer Genetics Program, Center for Cancer Research, National Cancer Institute, Frederick, MD 21702, USA

SUMMARY

The neural network of the temporal lobe is thought to provide a cognitive map of our surroundings. Functional analysis of this network has been hampered by coarse tools that often result in collateral damage to other circuits. We developed a chemogenetic system to temporally control electrical input into the hippocampus. When entorhinal input to the perforant path was acutely silenced, hippocampal firing patterns became destabilized and underwent extensive remapping. We also found that spatial memory acquired prior to neural silencing was impaired by loss of input through the perforant path. Together, our experiments show that manipulation of entorhinal activity destabilizes spatial coding and disrupts spatial memory. Moreover, we introduce a chemogenetic model for non-invasive neuronal silencing that offers multiple advantages over existing strategies in this setting.

*Correspondence: dji@bcm.edu (D.J.), jankowsk@bcm.edu (J.L.J.).

[9]Co-first author

SUPPLEMENTAL INFORMATION

Supplemental Information includes Supplemental Experimental Procedures, seven figures, four tables, and one movie and can be found with this article online at http://dx.doi.org/10.1016/j.celrep.2016.06.032.

AUTHOR CONTRIBUTIONS

R.Z., S.D.G., M.M.K., M.J.Y, A.L., T.-C.L., Y.J., and D.A.S. conducted the experiments. R.Z., S.D.G., M.M.K., Y.J., L.T., D.J., and J.L.J. designed the experiments. K.S. helped with statistical analyses. R.Z., S.D.G., D.J., and J.L.J wrote the manuscript.

In Brief

Zhao et al. present a chemogenetic model for acute neuronal silencing. Suppression of the entorhinal cortex causes remapping of hippocampal CA1 place fields and impairs recall of spatial memory. The concurrent disruption of place fields and spatial recall suggest that stable cognitive maps remain critical for navigation in a familiar setting.

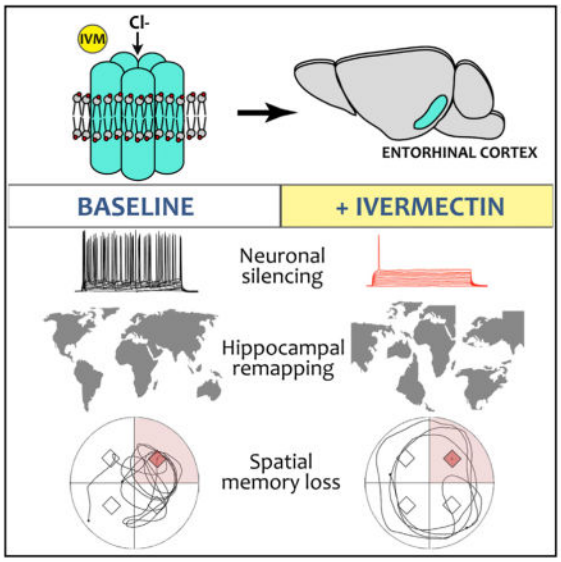

INTRODUCTION

During exploration of a novel environment, hippocampal neurons become responsive to specific locations, collectively generating a neural map for the new space. Their unique firing pattern offers a theoretical memory code for a particular environment, as well as a neural basis for recalling experiences associated with it. In this hypothesis, the same set of hippocampal neurons activated during initial exposure to a new space are used to support navigation on subsequent encounters. Several features of hippocampal place cells argue in favor of this hypothesis. First, some hippocampal place fields are stable for weeks or months, suggesting they encode long-term memory of a learned environment (Ziv et al., 2013). Second, place fields established during maze learning are sequentially reactivated before re-entering the maze, suggesting a reference map for successful navigation (Pfeiffer and Foster, 2013). Third, blocking consolidation of hippocampal firing sequences with NMDAR inhibitors impairs recall of goal-directed navigation, suggesting these unique firing patterns are essential for retrieval (Dupret et al., 2010).

Despite the appeal of a link between place field reactivation and spatial memory, experimental proof has been limited by the approaches available to dissect this complex circuit. Electrolytic and pharmacological lesions to inactivate cortical projections to the hippocampus impact spatial properties of CA1 neurons (Miller and Best, 1980; Brun et al., 2008; Van Cauter et al., 2008; Hales et al., 2014; Miao et al., 2015; Ormond and McNaughton, 2015; Schlesiger et al., 2015) and impair spatial learning (Good and Honey,

1997; Remondes and Schuman, 2004; Van Cauter et al., 2013; Hales et al., 2014). However, these lesioning methods have particular drawbacks in the entorhinal cortex where neurons in neighboring layers can have discrete targets and serve distinct functions. Such topographical precision requires genetic approaches capable of providing regional, layer, or cell-type specificity. Ideally, studies to functionally dissect the hippocampal-entorhinal network would harness both the topographic specificity of genetic approaches and the temporal precision of light- or ligand-activated channels. Here, we describe a transgenic system for neuronal silencing that meets these dual objectives. Our approach is based on a modified human glycine receptor (GlyCl) that is activated using the peripherally delivered ligand ivermectin (Lynagh and Lynch, 2010). The concept of this system is similar to other engineered receptors for neuronal silencing (i.e., PSAM or DREADDs) (Sternson and Roth, 2014), but uses an inexpensive and widely available drug for activation. By placing GlyCl expression under control of the tetracycline-transactivator (tTA), we can flexibly target neuronal populations by interbreeding with existing tTA driver lines. Here, we use one such tTA line to express GlyCl within the superficial entorhinal cortex. We show that the chemo-genetic suppression of neural activity in this model elicits dramatic remapping of hippocampal place fields and impairs recall of a trained location in a familiar environment. We thus introduce a model system for non-invasive dissection of circuit function that supports an operational correlation between spatial memory and hippocampal place field stability.

RESULTS

Transgenic Expression of an Engineered Chloride Channel for Reversible Suppression of Neuronal Firing

We sought to develop a chemogenetic approach for non-invasive neuronal silencing based on the human glycine-gated chloride channel (GlyCl). This homopentameric receptor had been optimized by Lynagh and Lynch (2010) for ligand-controlled neural silencing using inexpensive and readily available anti-parasitic avermectin drugs to activate a hyperpolarizing chloride current in mature neurons. Substitution at F207A reduced sensitivity for glycine, while a second substitution at A288G increased sensitivity for ivermectin (IVM). We used this F207A/A288G cDNA to create a transgenic construct in which two copies of the modified GlyCl channel and a YFP fluorescent indicator were placed under control of the tet-responsive promoter TRE3G (Figure 1A).

Placing GlyCl in the Entorhinal Cortex

The perforant pathway is the archetypal conduit for cortical information into the hippocampus, making it an obvious target for probing the link between successful recall of navigational memory and the stability of spatial tuning by hippocampal neurons. We crossed our TRE-GlyCl transgenic responder line to the EC-tTA driver line based on the neuropsin promoter (also known as Nop-tTA) (Yasuda and Mayford, 2006) to generate bigenic offspring expressing the IVM-sensitive GlyCl channel within the entorhinal cortex (hereafter abbreviated Nop-GlyCl). Although the Nop-tTA line is not specific for the entorhinal cortex (Yetman et al., 2016), the highest density of cells with strong YFP signal was found in the superficial medial entorhinal cortex and neighboring pre- and parasubiculum (Figure 1B). Axonal terminals of the perforant path were clearly visible by YFP labeling within the

molecular layer of the dentate gyrus (Figure 1C), confirming the layer 2 localization of transgene expression within entorhinal cortex. Although transgene expression was strongest in layer 2, YFP labeling was not found in all layer 2 neurons, nor was trans-gene expression fully excluded from other layers within this region. Immunostaining for GlyCl confirmed fidelity of the YFP label at the soma, with intense GlyCl immunostaining at the cell membrane and YFP more diffusely distributed throughout the cytoplasm (Figures 1D–1G). As expected from previous studies with this driver line (Yetman et al., 2016), moderate transgene expression was also seen in the deep layers of parietal association area, anterior cingulate cortex, and retrosplenial cortex, with sparse scattered YFP^+ cells across many other regions of the forebrain (Figure S1). Unexpectedly, cerebellar YFP expression appeared independent of tTA in single transgenic TRE-GlyCl mice and the bigenic Nop-GlyCl animals (Figure S1). A similar pattern of tTA-independent YFP labeling was seen in several other TRE-GlyCl founder lines created from the same construct (Figure S2; Table S1). This site of ectopic expression was notable because past studies have shown that chronic suppression of cerebellar LTD impairs spatial navigation based on self-motion cues (Rochefort et al., 2011; Lefort et al., 2015). With this in mind, we included GlyCl single transgenic animals as controls for all work with Nop-GlyCl mice to account for any cerebellar phenotypes that might influence our findings.

Neuronal Silencing with IVM In Vitro and In Vivo

We next confirmed that entorhinal GlyCl expression would render these neurons susceptible to IVM. We prepared acute brain slices for electrophysiology from 6- to 8-week-old Nop-GlyCl mice and single- or non-transgenic (NTG) control siblings. Pyramidal neurons in the entorhinal cortex (EC) were identified by fluorescence in Nop-GlyCl animals and by relative size and location in control animals. The frequency of action potentials evoked by stepped current injections in standard artificial cerebrospinal fluid (ACSF) showed no difference between control and Nop-GlyCl cells (Figures 2A–2C; Table S2; three-way ANOVA, main effect of genotype, $p < 0.0001$; post hoc Nop-GlyCl ACSF versus Control ACSF, $p = 0.2424$). Subsequent application of 100 nM IVM significantly reduced the resting membrane potential (unpaired t test, $p < 0.001$) and substantially impaired spike initiation only in GlyCl-expressing cells (three-way ANOVA, post hoc Nop-GlyCl ACSF versus Nop-GlyCl IVM, $p < 0.0001$). Supra-threshold stimulation elicited no action potentials in GlyCl-expressing neurons until 140 pA, and any spiking that did occur at higher intensities (180–200 pA) was at a greatly reduced rate compared to controls.

We next examined the impact of IVM-mediated silencing on synaptic transmission of entorhinal neurons through the perforant path. These recordings measured the slope of field excitatory postsynaptic potential (EPSPs) in the molecular layer of dentate gyrus following stimulation of the perforant path. In control animals, the stimulus-response relationship was unaffected by application of 100 nM IVM (Figure 2D; three-way ANOVA, genotype × treatment interaction, $p < 0.0001$; post hoc Control ACSF versus Control IVM, $p = 0.3360$). In contrast, IVM significantly depressed the stimulus-response curve in field recordings from Nop-GlyCl animals (three-way ANOVA, post hoc Nop-GlyCl ACSF versus Nop-GlyCl IVM, $p < 0.0001$). The magnitude of this change, ~43% ± 0.06% at plateau intensities between 300–400 μA, corresponded well with previous studies in which Nop-tTA was used

to express tetanus toxin in this region and with the same authors' estimate that 43% of superficial entorhinal neurons express tTA in this driver line (Yasuda et al., 2011)

IVM can be systemically administered by multiple routes, but brain concentration is limited by active efflux of the p-glycoprotein transporter (Geyer et al., 2009; Kiki-Mvouaka et al., 2010). We therefore examined the pharmacokinetics of IVM distribution in wild-type mice following a single intraperitoneal injection of 5 mg/kg. IVM concentration in the brain was near maximal by 3 hr post injection, peaked at 9 hr, then declined sharply with a $T_{1/2}$ of 13.3 hr (Figures 3A and 3B). The maximum brain concentration reached 65 ng IVM per gram brain weight, or 74 nM, approximately the concentration at which our whole-cell recordings in acute brain slices showed nearly complete inhibition of action potential initiation. We therefore administered IVM at 5 mg/kg intraperitoneal for all subsequent in vivo experiments.

We next used multi-tetrode recordings in awake behaving mice to examine the pharmacodynamics of IVM on neural activity in the brain following a single injection of IVM. For this experiment, we expressed GlyCl within hippocampal neurons using the CaMKIIα-tTA driver line to assess the direct effect of IVM-induced silencing on CA1 neurons. CA1 activity was continuously recorded for ~5 hr each day, allowing us to compare neural activity before and after IVM administration. On each day of recording, animals underwent three behavior sessions during which they ran laps on a linear track and then explored freely in open field, before they were returned to the home cage for 2 hr rest. On the first day, animals were injected with vehicle immediately after the baseline session and were returned to the track and open field for testing at 2 and 4 hr after injection. On the second day, IVM was substituted for vehicle in an otherwise identical protocol.

Multi-unit recordings revealed that the median firing rate in CaMKIIα-GlyCl mice did not change following vehicle injection, but decreased markedly within 2 hr of IVM treatment and declined still further by 4 hr, consistent with the pharmacokinetics of IVM in wild-type mice (Figures 3C and 3E; Kruskal-Wallis, $p = 0.0177$; post hoc baseline versus IVM 4 hr, $p = 0.0022$). The same temporal pattern was apparent in the single unit activity of many CA1 neurons (Figures 3D and 3F; Kruskal-Wallis, $p < 0.0001$; post hoc baseline versus IVM 2 hr, $p = 0.0004$; baseline versus IVM 4 hr, $p < 0.0001$). We further analyzed the single unit data using rate curves (Figure 3D, red traces) as a graphical depiction of the relationship between an animal's position on the linear track and the average firing rate of the cell. For each place cell identified, we computed between-session stability as a measure of how similar the firing rate curve was in the baseline session to those following treatment. Similar computations were done to assess between-session stability of two-dimensional rate maps in open field recordings. Compared with vehicle treatment the day before, direct silencing of CA1 neurons in the CaMKIIα-GlyCl mice sharply reduced the between-session stability both in open field exploration and on the linear track (Figure S3; Kruskal-Wallis, $p < 0.0001$; open field post hoc Vehicle versus IVM, $p < 0.0001$; linear track post hoc Vehicle versus IVM, $p < 0.0001$).

Pharmacogenetic Silencing of Superficial EC Disrupts Spatial Tuning in CA1

Returning to the Nop-GlyCl mice, we expected IVM administration to diminish the amplitude and disrupt the patterning of transmission through the perforant path and predicted that this change might influence the spatial tuning of downstream CA1 neurons. Because IVM administration had an equivalent effect on place field stability in CaMKII-GlyCl mice regardless of whether we recorded on a one-dimensional linear track or a two-dimensional open field (Figure S3), we opted to use the more reliable linear track measures for all subsequent analyses. Further, animals show a clear improvement in track performance with continued days of training, suggesting that track running for food reward is a learned behavior (Figure S4; two-way repeated measure (RM) ANOVA, main effect of day, $p < 0.0001$; post hoc day 1, 2 versus day 6, 7, $p < 0.0001$ for all comparisons, all genotypes). We tested three groups of mice in this experiment: Nop-GlyCl bigenic animals, GlyCl single transgenic animals, and a control group comprised of both NTG and tTA single transgenic animals. Similar to the previous protocol, CA1 activity was continuously recorded throughout the ~5 hr experiment and compared between three track running sessions: baseline, 2 hr, and 4 hr after systemic administration of either vehicle or IVM. Between-session stability approached 0.6 for all three groups and was unchanged by IVM injection in the control and GlyCl single transgenic groups (Figure 4A). However, IVM treatment in the Nop-GlyCl mice precipitated a dramatic decline in the between-session stability (Figures 4A and S5; Kruskal-Wallis, $p < 0.0001$; post hoc vehicle versus IVM, $p < 0.0001$). The relative order, peak rate, and firing position for each cell remained relatively consistent between baseline and 4 hr after vehicle injection (Figure 4B), but were severely disrupted by IVM in the Nop-GlyCl mice (Figure 4C). Compared to the highly consistent location of place fields observed in control mice after either vehicle or IVM injection (Figures 4D and 4E), place fields in Nop-GlyCl mice remained stable and well-defined after vehicle injection (Figure 4F) but often appeared more diffuse or became active in new locations following IVM injection (Figure 4G). In some cases, cells that were active during baseline became silent after IVM, and in others, cells that were silent developed well-defined place fields.

We next examined what factors contributed to the decline in rate map correlation following IVM administration in the Nop-GlyCl model. We began by comparing spatial information (SI) between sessions, which offers a measure of how unambiguously the firing of each place cell reflects the position of the animal. The SI provided by CA1 neurons was unchanged by IVM injection in control and GlyCl groups, but was significantly reduced in Nop-GlyCl mice (Figure 5A; Tables S2 and S3; Kruskal-Wallis, $p < 0.0001$; post hoc baseline versus IVM 2 hr, $p = 0.0003$; baseline versus IVM 4 hr, $p = 0.0016$). In concert with this change in SI, the average length represented by each place field increased significantly in the IVM-treated Nop-GlyCl mice (Figure 5B; two-way ANOVA, genotype × treatment interaction, $p < 0.0001$; post hoc baseline versus IVM 2 hr and versus IVM 4 hr, $p < 0.0001$). These changes occurred without any decline in overall firing rate: both multi-unit and aggregate single unit activity were stable across days and between sessions for all genotypes (Figures S6A and S6B). Moreover, the average and peak firing rates of putative pyramidal neurons were unchanged (Figures S6D and S6E). In contrast to past studies of entorhinal lesions (Bragin et al., 1995; Schlesiger et al., 2015), we found no change in theta power between sessions on either day of testing (Figures S6C and S6G). This discrepancy is likely

due to the limited targeting of layer 2 neurons with the Nop-tTA driver (40%–50%) compared with the near-total cell loss produced by physical lesions in the earlier studies. Similarly, although past studies have shown a relationship between run speed and CA1 theta power (Long et al., 2015), the slowing of Nop-GlyCl mice after IVM may have been too small to significantly impact theta amplitude here (Figure S6F). IVM silencing had no impact on the proportion of cells with place fields nor in the number of place fields per cell (Table S4). The increase in field size clearly contributed to the drop in SI, but analysis of rate curves from Nop-GlyCl mice before and after IVM indicate that positional stability was also a factor.

To better understand the nature of place field instability caused by IVM silencing, we categorized cells as remaining stable if neither peak firing rate nor position changed between sessions; as undergoing rate modulation if firing rate, but not place field location, differed; or as undergoing global remapping if place field location was altered (Figure 6A). The fraction of cells in each category was similar between genotypes after vehicle administration (Figure 6B; three-way ANOVA, genotype × treatment × classification, $p = 0.00496$). In IVM-treated Nop-GlyCl mice, however, stable place cells decreased by more than two-thirds (post hoc vehicle versus IVM, $p = 0.1123$) while the number of cells that underwent global remapping increased 3-fold (post hoc vehicle versus IVM, $p = 0.0251$). These experiments prove that disruption of entorhinal input to the hippocampus—either on its own or in addition to the disruption of activity in several other areas where GlyCl was expressed—significantly destabilizes spatial tuning of CA1 pyramidal neurons.

Navigation in a Familiar Environment Is Impaired following Disruption of Entorhinal Input to Hippocampus

Having established a model in which we could experimentally induce global remapping of CA1 place fields, we next tested whether the same manipulation of entorhinal activity would impact spatial navigation. We observed no differences in locomotion or anxiety between genotypes in open field or straight swim training (Figure S7) and so proceeded with Morris water maze (MWM) training. The MWM task allowed us to overcome the unanticipated scratching behavior caused by IVM in the Nop-GlyCl mice. This behavior was never observed in control animals and was most apparent during place cell recording as animals paused at each end of the track for food reward. This period of inactivity is excluded from analysis for all animals and thus did not affect place cell measurements. Because mice cannot scratch and swim at the same time, the use of MWM eliminated this confound from our behavioral testing.

We previously validated a modified version of the MWM in which learning is assessed at the end of each day using a short-term memory probe, and training continues for each mouse until it reaches pre-fixed success criteria (Fowler et al., 2014). Using this protocol, all four genotypes learned the location of the hidden platform in the water maze, although the Nop-GlyCl group took more training to master the task than GlyCl single transgenic animals (Figure 7A; Kruskal-Wallis, $p = 0.0211$; post hoc GlyCl versus Nop-GlyCl, $p = 0.0319$) and swam significantly farther during the initial days of training than controls (Figure 7B; two-way RM ANOVA, main effect of genotype, $p = 0.0415$, all post hoc comparisons n.s.). This

delay in acquisition may have resulted from GlyCl expression during postnatal development of the perforant pathway and suggests that future studies may benefit from rearing animals on doxycycline to withhold trans-gene expression until adulthood. After reaching criteria, animals were retired from further training until the last mouse had finished, and the next day all animals underwent a single day of refresher training to ensure equivalent performance across groups prior to long-term memory assessment. Although the Nop-GlyCl mice had taken more days to learn the task, they performed as well as controls during refresher training (one-way ANOVA, path length $p = 0.5710$) and during the probe trial immediately following refresher training (one-way ANOVA, % path in trained quadrant $p = 0.9376$; proximity to phantom platform, $p = 0.3392$).

After confirming that all mice had learned the task equally well, we then tested whether long-term spatial memory was disrupted concurrent with CA1 remapping. The day after refresher training, mice were injected with vehicle solution and 3 hr later underwent a single probe trial to assess spatial recall. As expected from the design of this task, all four genotypes performed equally well following vehicle injection, displaying equivalent proximity to the phantom platform (Figure 7E; two-way RM ANOVA, treatment × genotype interaction, $p < 0.0001$, all post hoc genotype comparisons after vehicle injection were n.s. [in contrast to the IVM response described below]). Examples of the swim paths taken by mice from each genotype during this post-vehicle probe test clearly favor the trained northeast quadrant of the pool (Figure 7C; Movie S1) and average percent of swim path within the target quadrant was similar for all four genotypes (40%–45%; Figure 7D; two-way RM ANOVA, treatment × genotype interaction $p = 0.0073$, all post hoc genotype comparisons after vehicle injection were n.s [again, in contrast to IVM response described below]). Thus by all measures, spatial recall in the Nop-GlyCl group was equivalent to the control groups under vehicle conditions.

We next tested the impact of IVM silencing on spatial recall in this now-familiar environment. All mice first received one final training session to prevent memory extinction by prior probe testing. The following day, animals were injected with IVM and 3 hr later underwent a second probe test for long-term spatial memory. In contrast to IVM-treated control animals, the swim paths of IVM-treated Nop-GlyCl mice showed little or no preference for the trained quadrant (Figure 7C). Following IVM administration, Nop-GlyCl animals occupied the trained quadrant significantly less and focused their search for the phantom platform with significantly lower precision than they had following vehicle injection (two-way RM ANOVA for % path, treatment × genotype interaction, $p = 0.0073$, post hoc Nop-GlyCl vehicle versus IVM $p = 0.0061$; two-way RM ANOVA for proximity, treatment × genotype interaction, $p < 0.0001$, post hoc Nop-GlyCl vehicle versus IVM $p < 0.0001$). To rule out the possibility that the navigational effect of neuronal silencing was caused by non-specific impairments in visual acuity or swimming ability, we performed a visible cue variation of the water maze immediately after completing the IVM probe trial. Because the average path length swum by Nop-GlyCl mice in the visible platform trials was longer than other IVM-treated groups (Figure S7G; one-way ANOVA, $p = 0.0237$, all post hoc comparisons were n.s.), we looked more carefully at the individual trial data. This analysis revealed a main effect of genotype for path length, but none of the post hoc comparisons were significant for any quadrant tested (Figure S7I; two-way RM ANOVA,

main effect of genotype, $p = 0.0214$). We conclude from these analyses that the IVM-treated Nop-GlyCl mice were capable of swimming to a well-defined target as efficiently as controls, however, they appeared to do so less consistently than controls. This may reflect inflexibility for changing task demands rather than visual or attentional impairment. Collectively these findings suggest that spatial recall relies on continued entorhinal input, stable CA1 positional tuning, or both, even within a familiar environment.

DISCUSSION

Despite remarkable progress in analyzing circuits that support spatial tuning in the hippocampus, methods for experimentally manipulating elements of this system have been comparatively limited. Here, we introduce a transgenic model that allows spatial control over neuronal activity in navigational circuits in a behaviorally relevant time frame. The GlyCl-ivermectin approach described here has several advantages over existing systems such as optogenetics, DREADDs, and PSAMs for neuro-functional studies (Sternson and Roth, 2014). The GlyCl channel is activated by a systemically delivered ligand amenable to use in widely dispersed neural populations or regions difficult to implant with fiber optics and does not require intracellular second messengers for its function. Ivermectin is widely available and well-characterized. Activation of endogenous mammalian receptors can occur at high doses (Wolstenholme, 2010; Zemkova et al., 2014), but with more than a dozen avermectin and milbemycin variants available, alternative ligands may emerge to improve brain penetrance and minimize off-target modulation (Shoop et al., 1995; Prichard et al., 2012).

Our work builds on a longstanding quest to define the relationship between hippocampal place fields and spatial memory. Previous studies showed that the dynamic realignment between environmental landmarks and CA1 tuning was critical for successful navigation and that animals were more likely to make navigational errors during when changes in external cues caused place fields to shift between training and testing (O'Keefe and Speakman, 1987; Lenck-Santini et al., 2001). Subsequent studies revealed that spatial learning deficits characteristic of aging rodents were associated with diminished place field stability in familiar locations and ineffective remapping in novel environments (Barnes et al., 1997; Tanila et al., 1997; Oler and Markus, 2000; Wilson et al., 2003). Consistent with the idea that place fields are essential to encoding spatially anchored information, recent work has shown that events encountered within a place field (such as food reward or foot shock) can cause place field remapping and that tuning patterns generated during acquisition become reactivated during recall of the rewarded trajectory (Anderson and Jeffery, 2003; Moita et al., 2003, 2004; Smith and Mizumori, 2006; Dupret et al., 2010). Our work builds on this foundation by showing that a single experimental manipulation can both destabilize spatial tuning in CA1 and impair recall of established spatial memory. Because we used entorhinal silencing to evoke CA1 instability, our current model cannot disambiguate the contribution of CA1 instability and entorhinal inactivation to spatial memory impairments. The extensive bidirectional connections between entorhinal cortex and hippocampus may ultimately prevent the two regions from being separated experimentally in a meaningful way. This consideration applies broadly to any experimental system designed to "selectively manipulate" neurons within a highly interconnected network, but is especially pertinent within the temporal lobe. Despite these caveats of circuit manipulation, our findings support

an experimental correlation between entorhinal output, hippocampal place field stability, and reliable navigation of a known context.

Fundamental to our study was the discovery that neuronal silencing in the Nop-GlyCl mice induced extensive remapping of CA1 place fields. Past studies had shown that physical or chemical lesions of the entorhinal cortex diminished the stability of CA1 place fields, increased field size, and reduced the density of spatial information provided by each cell (Miller and Best, 1980; Van Cauter et al., 2008; Hales et al., 2014; Schlesiger et al., 2015). Here, we confirm these effects and further demonstrate through continuous recordings that extensive CA1 remapping occurs in real time following entorhinal silencing. This outcome adds to several recent reports in models of optogenetic, chemogenetic (DREADD), or pharmacologic (muscimol) inactivation of MEC, where both CA1 and CA3 place fields were found to undergo extensive destabilization and expansion within tens of minutes following onset (Miao et al., 2015; Ormond and McNaughton, 2015; Rueckemann et al., 2016). In contrast to these models where stereotaxic injection of drug or virus biased MEC inactivation toward dorsal or ventral populations but spanned all cortical layers, we show that genetically isolating MEC layer 2 had the same effect. Surprisingly, while these studies of direct MEC inactivation support a strong influence on hippocampal spatial tuning, more subtle manipulations to specifically dampen entorhinal grid firing have reported little impact on the positional stability of CA1 place fields (Koenig et al., 2011; Brandon et al., 2014). This difference may simply reflect the likelihood that CA1 place fields are shaped by many types of feature-, positional-, proprioceptive-, and vestibular-responsive cells in the entorhinal area and may be robust to the specific loss of grid cell input.

It is also important to note that the Nop-tTA driver also induces transgene expression in superficial layers of retrosplenial cortex, a region that contains head direction cells which contribute to positional tuning of CA1 neurons and to spatial navigation. However, past work shows that while acute silencing of retrosplenial cortex destabilizes hippocampal place fields and diminishes initial search precision during probe trials, loss of retrosplenial input was not sufficient to impair spatial navigation as long as environmental cues were visible (Cooper and Mizumori, 1999, 2001; Czajkowski et al., 2014). Therefore, loss of retrosplenial function is unlikely to cause the dramatic spatial memory impairment evoked by ivermectin in the Nop-GlyCl mice, but this warrants confirmation through future studies in which GlyCl expression is strictly limited to the entorhinal cortex.

Another complication of the current model is the unexplained scratching elicited by ivermectin administration in Nop-GlyCl mice. The effect was selective to bigenic animals, occurred in multiple TRE-GlyCl founder lines crossed to the Nop driver (data not shown) and persisted even when the GlyCl transgene was introduced specifically to the CNS by viral expression (data not shown). Scratching abated over several days, which is somewhat longer than the pharmacokinetics of ivermectin clearance, but not inconsistent with drug perdurance in lipid membranes. We tested spatial recall in the water maze because swimming prevented the mice from scratching during the task. Nevertheless, the feeling of itch could have distracted attention from the task, leading to a drop in place field stability (Kentros et al., 2004; Muzzio et al., 2009). However, ivermectin treatment affected multiple field parameters not yet linked to attention, including firing rate, field size, and spatial

information, suggesting that diminished attention was not likely responsible for the extensive remapping we observed.

Admittedly, the linear track task used for place field analysis may have had different attentional demands than the water maze used to assess behavioral consequences of neuronal silencing. Both track running in return for food reward and water maze navigation are learned tasks, suggesting that both require some degree of attention to master. However, once the shape and setting of the track become familiar, successful navigation may become more automatic than for the water maze where variable start points and directional freedom require active engagement with visible cues for guidance. Thus, it is possible that the extent of remapping observed on a linear track may be greater than in the water maze. However, even if the higher attentional requirements of water maze testing lessened the impact on place field size, stability, spatial information, and firing rate, the changes that did occur were sufficient to cut spatial memory performance down to chance levels.

Recognizing these caveats, our study nevertheless demonstrates that the same acute disruption of entorhinal activity was sufficient to both destabilize spatial tuning of CA1 place fields and impair recall of established spatial memory. We are optimistic that genetic tools such as the GlyCl channel described here will transform how spatial navigation circuits are investigated and will soon move the field from correlation to a causal link between hippocampal activity sequences and subsequent recall of places from which they arose.

EXPERIMENTAL PROCEDURES

For detailed description, see the Supplemental Experimental Procedures.

Mice

TRE-GlyCl—The GlyCl coding cassette was engineered to contain the fluorescent reporter from pEYFP-N1 (Clontech), flanked on either side by human GlyClα harboring the F207A/A288G point mutations (Lynagh and Lynch, 2010), separated by T2A peptide sequences (Trichas et al., 2008), and followed by a woodchuck hepatitis post transcriptional regulatory element (WPRE) (Lerchner et al., 2007). This cassette was ligated into the moPrp-TRE3G vector (modified from Jankowsky et al., 2005) to build moPrp-TRE3G-GlyClα-2A-YFP-2A-Gly-Clα-WPRE (abbreviated hereafter as TRE-GlyCl; Figure 1A). Mice harboring the TRE-GlyCl construct were generated using standard techniques for pronu-clearinjection and screened for transgene expression using YFP expression and IVM sensitivity. TRE-GlyCl line 9542 was backcrossed to FVB/NJ for a minimum of three generations before being mated with tTA driver lines described below. Line 9542 is available from the Jackson Laboratory as stock #29302; additional lines generated from the same construct are also available and described in Supplemental Information. Both male and female TRE-GlyCl mice were used for breeding, yielding offspring on a mixed hybrid background derived from C3H, C57, and FVB strains. All animal experiments were reviewed and approved by the Baylor College of Medicine International Care and Use Committee.

Neuropsin-tTA—Mice expressing a humanized tTA under control of the mouse neuropsin (Nop)/ protease serine 19 (Prss19)/Kallikrein-related peptidase 8 (Klk8) promoter were generously provided by Dr. Mark Mayford (Line tTA-EC) (Yasuda and Mayford, 2006) (available from MMRRC as stock #31779). The line was backcrossed to C57BL/6 for at least four generations before being mated with TRE-GlyCl for these studies.

CaMKIIα-tTA—CaMKIIα-TTA line B mice expressing the tetracycline transactivator (TTA) under control of the calcium-calmodulin kinase type IIα (CaMKIIα) promoter (Jackson Laboratories #3010) (Mayford et al., 1996) were used to create bigenic CaMKII-GlyCl offspring. This line had been backcrossed to C57BL/6J for >20 generations prior to use in GlyCl matings for this study.

Drugs—For all in vivo experiments, Ivomec (1% ivermectin injectable solution, Merial) was diluted to 0.2% with vehicle (3:2 mix of propylene glycol and 0.9% saline). Stock dilutions were made fresh on the day of injection and administered at 5 mg/kg intraperitoneally (i.p.). For in vitro electrophysiology studies, Ivermectin powder (Sigma-Aldrich I8898) was dissolved in DMSO at a stock concentration of 100 μM, stored at −20°C for up to 1 week and diluted daily to 100 nM with ACSF for the final working solution.

Brain Slice Electrophysiology—Whole-cell voltage-clamp recordings of layer 2 entorhinal neurons were performed in acute brain slices to measure the number of action potentials generated in response to 500 ms current injections (−60 pA to 200 pA at 20 pA increments). Throughout the experiment, access resistance was 10–35 MΩ and cells were discarded if R_a drifted above 20%. Current-response relationships were constructed by counting the number of action potentials generated at each current step in the presence or absence of IVM.

In separate set of experiments, field excitatory postsynaptic potential (fEPSP) responses were recorded in the medial molecular layer of the dentate gyrus following perforant path stimulation. Stimulus-response relationships were calculated by plotting initial slope of the fEPSPs against stimulus intensity, first in normal ACSF, then following addition of 100 nM IVM.

IVM Pharmacokinetics—Twelve-week-old adult ICR mice were injected with IVM and killed by pentobarbital overdose between 3 hr to 4 days later. At each time point, four mice (two males [M], two females [F]) were used for cardiac puncture and brain dissection. Blood was collected into heparinized tubes and spun at 3,000 rpm for 15 min at 4°C to isolate the plasma which was then snap frozen. Brain tissue was extracted without perfusion, dissected along the midline, and frozen on dry ice. The IVM concentrations in plasma and brain samples were quantitated using validated liquid chromatography-tandem mass spectrometry methods.

In Vivo Multi-tetrode Recordings—A craniotomy was made at −2.0 mm posterior and 1.5 mm lateral from bregma to insert the drive cannula and position the tetrodes just above the cortex. Animals were given a week to recover before being placed on food restriction to maintain 85% of their projected ad libitum body weight. Animals were trained

for ~3 weeks to run laps forward and back for a food reward along a ~2 m long rectangular track. During training, chronically implanted tetrodes were slowly lowered into the pyramidal layer of dorsal CA1 using the appearance of ripples in the local field potential to identify the correct placement. A tetrode placed in the cortex was used as the reference electrode. A metal screw was implanted in the skull over the cerebellum to serve as the ground.

Recording began when the animals could reliably run at least ten laps in each direction and multiple stable hippocampal CA1 neurons could be isolated as single-units. Details of recording procedures and data analysis have been described previously (Ji and Wilson, 2007; Cheng and Ji, 2013). Tetrode recordings were acquired using a DigitaLynx system (Neuralynx). Extracellular voltage signals from four channels in each tetrode were digitized at 32 kHz and band-pass filtered between 600 Hz and 9 kHz. Spikes were counted when the voltage signal from any of the channels surpassed a trigger threshold of 50–70 μV. Broadband local field potentials of 0.1 Hz–1 kHz were sampled at 2 kHz. Single neurons were manually isolated using xclust (Matthew Wilson, MIT).

Place Field Analysis—Active putative pyramidal neurons with a mean firing rate between 0.5 and 7 Hz during any one of the three recording sessions were used to calculate mean firing rate. Thus, any cell that had a mean rate of 0.5 to 7 Hz during one session was also included in the calculation of mean firing rate for the remaining sessions. This ensured that our analysis captured cells that underwent significant changes in firing rate following IVM injection. For the calculation of place field length and peak firing rate, only cells with a peak rate >1 Hz, a mean rate >0.5 Hz and field length >10 cm on every session for that day of recording were included. Thus, field length and peak rate calculations were based on a subset of the total cells used for analysis of mean firing rate. Tentative place fields were defined from the peak(s) in the rate curve for each cell active on a trajectory. A threshold of 10% peak firing rate was used as the cutoff for place field boundaries. By this method, the field began from the first point at which the rate curve crossed above 10% peak rate and ended where it later crossed below 10% peak rate. The field length was calculated as the linear distance between these boundaries. Neighboring fields separated by <4 cm were combined into a single field.

Place Field Categorization—A place cell was classified as stable if its (1) place field location did not shift, reflected by a significant correlation between rate curves obtained during baseline and 4 hr post injection ($p < 0.05$, Pearson's r), and (2) peak firing rate at 4 hr was between 0.5 and 2 times of peak rate during the baseline session. A cell was classified as rate modulated if its (1) place field location did not shift across sessions, and (2) peak firing rate at 4 hr was <0.5 or more than 2 times of peak rate during the baseline session. A cell was classified as globally remapped if it (1) displayed a place field during the baseline session that disappeared at 4 hr, or (2) was silent during baseline and became active at 4 hr, or (3) shifted firing location between the baseline and 4-hr sessions.

Multi-unit Activity Analysis—Sharp wave amplitude was assessed for each tetrode during the baseline recording session and again after IVM injection. Only tetrodes with amplitude changes of <20% across sessions were used for analysis. Multi-unit activity

(MUA) spikes were counted in 10-ms bins for all periods of running during each track session. The MUA rate was defined as the total number of spikes divided by the total time spent running. The MUA rate measured during the baseline recording session was used to normalize rates measured during the post injection sessions on each day.

Behavioral Assays—Mice aged to 3 months were handled for 3 days prior to the start of behavioral testing, which began with an open field test to assess locomotor activity, followed by MWM to assess spatial reference memory, ending with cued water maze testing to confirm visual acuity. Trials were recorded and tracked using ANY-maze Video Tracking System. Prior to the start of Morris water maze training, mice received 1 day of training in a straight swim channel to acclimate them to the water and check for motor deficits. Acquisition and refresher training in the MWM consisted of 4 trials/day with a 15 min ITI followed by a 45 s short-term memory probe without the platform. Mice were retired from training once they met two performance criteria during the probe trial: first, ≥40% of their total swim path had to be located in the trained quadrant, and second, their platform crossings over the trained location had to be at least two times more than each of the three other equivalent sites (NW, SW, SE) within the pool. Mice that did not reach criteria after 10 days of training were eliminated from further testing (n = 1 Nop and 3 Nop-GlyCl animals). Visual acuity testing was performed with a submerged platform marked with a high-contrast striped pole that was initially placed in the same quadrant as during training (NE) and then moved in pseudo-random order to a new site so that all four intermediate cardinal points were tested.

Statistics—Statistic comparisons used are described within the results; full details for main statistical comparisons are shown in Table S2. Prism 6.0 software (GraphPad) was used for all statistical analyses, with the exception of three-way ANOVA which used R software (version 3.2.4). Statistical analyses were designed to compare treatment within genotype, unless otherwise specified. Wherever possible, data that was normally distributed was plotted using mean ± SEM. In the case of non-normal distributions, data have been plotted using median ± interquartile ranges as appropriate for non-parametric data-sets. Significance values indicated in figures are for post hoc comparisons and use standard nomenclature: *$p < 0.05$, **$p < 0.01$, ***$p < 0.001$, and ****$p < 0.0001$.

Supplementary Material

Refer to Web version on PubMed Central for supplementary material.

Acknowledgments

We thank Henry Lester for initially harnessing cys-loop receptors for neuronal silencing, Timothy Lynagh and Joseph Lynch for sharing their optimized F207A/A288G GlyCl cDNA, Roy Sillitoe for expert guidance on cerebellar anatomy, Mark Mayford and Karsten Baumgartel for sharing the Nop-tTA line, Hunter Allen for assistance screening founder lines, and Bryan Song and Rebecca Corrigan for excellent care of the animal colony. This work was funded by an NIH Director's New Innovator Award DP2 OD001734 (J.L.J.), R21 MH101583 (J.L.J.), T32 AG000183 (support for S.D.G. and M.J.Y.), Bright-Focus Foundation postdoctoral fellowship A2015016F (S.D.G.), a gift from the Gillson Longenbaugh Foundation, and seed funds from Baylor College of Medicine (J.L.J.). D.A.S. and L.T. were supported by the Intramural Research Program of the NIH, National Cancer Institute, Center for Cancer Research.

References

O'Keefe J, Speakman A. Single unit activity in the rat hippocampus during a spatial memory task. Exp Brain Res. 1987; 68:1–27. [PubMed: 3691688]

Zemkova H, Tvrdonova V, Bhattacharya A, Jindrichova M. Allosteric modulation of ligand gated ion channels by ivermectin. Physiol Res. 2014; 63(Suppl 1):S215–S224. [PubMed: 24564661]

Anderson MI, Jeffery KJ. Heterogeneous modulation of place cell firing by changes in context. J Neurosci. 2003; 23:8827–8835. [PubMed: 14523083]

Barnes CA, Suster MS, Shen J, McNaughton BL. Multistability of cognitive maps in the hippocampus of old rats. Nature. 1997; 388:272–275. [PubMed: 9230435]

Bragin A, Jandó G, Nádasdy Z, Hetke J, Wise K, Buzsáki G. Gamma (40–100 Hz) oscillation in the hippocampus of the behaving rat. J Neurosci. 1995; 15:47–60. [PubMed: 7823151]

Brandon MP, Koenig J, Leutgeb JK, Leutgeb S. New and distinct hippocampal place codes are generated in a new environment during septal inactivation. Neuron. 2014; 82:789–796. [PubMed: 24853939]

Brun VH, Leutgeb S, Wu HQ, Schwarcz R, Witter MP, Moser EI, Moser MB. Impaired spatial representation in CA1 after lesion of direct input from entorhinal cortex. Neuron. 2008; 57:290–302. [PubMed: 18215625]

Cheng J, Ji D. Rigid firing sequences undermine spatial memory codes in a neurodegenerative mouse model. eLife. 2013; 2:e00647. [PubMed: 23805379]

Cooper BG, Mizumori SJ. Retrosplenial cortex inactivation selectively impairs navigation in darkness. Neuroreport. 1999; 10:625–630. [PubMed: 10208601]

Cooper BG, Mizumori SJ. Temporary inactivation of the retrosplenial cortex causes a transient reorganization of spatial coding in the hippocampus. J Neurosci. 2001; 21:3986–4001. [PubMed: 11356886]

Czajkowski R, Jayaprakash B, Wiltgen B, Rogerson T, Guzman-Karlsson MC, Barth AL, Trachtenberg JT, Silva AJ. Encoding and storage of spatial information in the retrosplenial cortex. Proc Natl Acad Sci USA. 2014; 111:8661–8666. [PubMed: 24912150]

Dupret D, O'Neill J, Pleydell-Bouverie B, Csicsvari J. The reorganization and reactivation of hippocampal maps predict spatial memory performance. Nat Neurosci. 2010; 13:995–1002. [PubMed: 20639874]

Fowler SW, Chiang AC, Savjani RR, Larson ME, Sherman MA, Schuler DR, Cirrito JR, Lesné SE, Jankowsky JL. Genetic modulation of soluble Aβ rescues cognitive and synaptic impairment in a mouse model of Alzheimer's disease. J Neurosci. 2014; 34:7871–7885. [PubMed: 24899710]

Geyer J, Gavrilova O, Petzinger E. Brain penetration of ivermectin and selamectin in mdr1a,b P-glycoprotein- and bcrp- deficient knockout mice. J Vet Pharmacol Ther. 2009; 32:87–96. [PubMed: 19161460]

Good M, Honey RC. Dissociable effects of selective lesions to hippocampal subsystems on exploratory behavior, contextual learning, and spatial learning. Behav Neurosci. 1997; 111:487–493. [PubMed: 9189263]

Hales JB, Schlesiger MI, Leutgeb JK, Squire LR, Leutgeb S, Clark RE. Medial entorhinal cortex lesions only partially disrupt hippocampal place cells and hippocampus-dependent place memory. Cell Rep. 2014; 9:893–901. [PubMed: 25437546]

Jankowsky JL, Slunt HH, Gonzales V, Savonenko AV, Wen JC, Jenkins NA, Copeland NG, Younkin LH, Lester HA, Younkin SG, Borchelt DR. Persistent amyloidosis following suppression of Abeta production in a transgenic model of Alzheimer disease. PLoS Med. 2005; 2:e355. [PubMed: 16279840]

Ji D, Wilson MA. Coordinated memory replay in the visual cortex and hippocampus during sleep. Nat Neurosci. 2007; 10:100–107. [PubMed: 17173043]

Kentros CG, Agnihotri NT, Streater S, Hawkins RD, Kandel ER. Increased attention to spatial context increases both place field stability and spatial memory. Neuron. 2004; 42:283–295. [PubMed: 15091343]

Kiki-Mvouaka S, Ménez C, Borin C, Lyazrhi F, Foucaud-Vignault M, Dupuy J, Collet X, Alvinerie M, Lespine A. Role of P-glycoprotein in the disposition of macrocyclic lactones: A comparison

between ivermectin, eprinomectin, and moxidectin in mice. Drug Metab Dispos. 2010; 38:573–580. [PubMed: 20089736]

Koenig J, Linder AN, Leutgeb JK, Leutgeb S. The spatial periodicity of grid cells is not sustained during reduced theta oscillations. Science. 2011; 332:592–595. [PubMed: 21527713]

Lefort JM, Rochefort C, Rondi-Reig L. Group of L.R.R. is member of Bio-Psy Labex and ENP Foundation. Cerebellar contribution to spatial navigation: new insights into potential mechanisms. Cerebellum. 2015; 14:59–62. [PubMed: 25630873]

Lenck-Santini PP, Save E, Poucet B. Evidence for a relationship between place-cell spatial firing and spatial memory performance. Hippocampus. 2001; 11:377–390. [PubMed: 11530842]

Lerchner W, Xiao C, Nashmi R, Slimko EM, van Trigt L, Lester HA, Anderson DJ. Reversible silencing of neuronal excitability in behaving mice by a genetically targeted, ivermectingated Cl-channel. Neuron. 2007; 54:35–49. [PubMed: 17408576]

Long LL, Bunce JG, Chrobak JJ. Theta variation and spatiotemporal scaling along the septotemporal axis of the hippocampus. Front Syst Neurosci. 2015; 9:37. [PubMed: 25852496]

Lynagh T, Lynch JW. An improved ivermectin-activated chloride channel receptor for inhibiting electrical activity in defined neuronal populations. J Biol Chem. 2010; 285:14890–14897. [PubMed: 20308070]

Mayford M, Bach ME, Huang YY, Wang L, Hawkins RD, Kandel ER. Control of memory formation through regulated expression of a CaMKII transgene. Science. 1996; 274:1678–1683. [PubMed: 8939850]

Miao C, Cao Q, Ito HT, Yamahachi H, Witter MP, Moser MB, Moser EI. Hippocampal Remapping after Partial Inactivation of the Medial Entorhinal Cortex. Neuron. 2015; 88:590–603. [PubMed: 26539894]

Miller VM, Best PJ. Spatial correlates of hippocampal unit activity are altered by lesions of the fornix and endorhinal cortex. Brain Res. 1980; 194:311–323. [PubMed: 7388617]

Moita MA, Rosis S, Zhou Y, LeDoux JE, Blair HT. Hippocampal place cells acquire location-specific responses to the conditioned stimulus during auditory fear conditioning. Neuron. 2003; 37:485–497. [PubMed: 12575955]

Moita MA, Rosis S, Zhou Y, LeDoux JE, Blair HT. Putting fear in its place: remapping of hippocampal place cells during fear conditioning. J Neurosci. 2004; 24:7015–7023. [PubMed: 15295037]

Muzzio IA, Levita L, Kulkarni J, Monaco J, Kentros C, Stead M, Abbott LF, Kandel ER. Attention enhances the retrieval and stability of visuospatial and olfactory representations in the dorsal hippocampus. PLoS Biol. 2009; 7:e1000140. [PubMed: 19564903]

Oler JA, Markus EJ. Age-related deficits in the ability to encode contextual change: a place cell analysis. Hippocampus. 2000; 10:338–350. [PubMed: 10902903]

Ormond J, McNaughton BL. Place field expansion after focal MEC inactivations is consistent with loss of Fourier components and path integrator gain reduction. Proc Natl Acad Sci USA. 2015; 112:4116–4121. [PubMed: 25733884]

Pfeiffer BE, Foster DJ. Hippocampal place-cell sequences depict future paths to remembered goals. Nature. 2013; 497:74–79. [PubMed: 23594744]

Prichard R, Ménez C, Lespine A. Moxidectin and the avermectins: Consanguinity but not identity. Int J Parasitol Drugs Drug Resist. 2012; 2:134–153. [PubMed: 24533275]

Remondes M, Schuman EM. Role for a cortical input to hippocampal area CA1 in the consolidation of a long-term memory. Nature. 2004; 431:699–703. [PubMed: 15470431]

Rochefort C, Arabo A, André M, Poucet B, Save E, Rondi-Reig L. Cerebellum shapes hippocampal spatial code. Science. 2011; 334:385–389. [PubMed: 22021859]

Rueckemann JW, DiMauro AJ, Rangel LM, Han X, Boyden ES, Eichenbaum H. Transient optogenetic inactivation of the medial entorhinal cortex biases the active population of hippocampal neurons. Hippocampus. 2016; 26:246–260. [PubMed: 26299904]

Schlesiger MI, Cannova CC, Boublil BL, Hales JB, Mankin EA, Brandon MP, Leutgeb JK, Leibold C, Leutgeb S. The medial entorhinal cortex is necessary for temporal organization of hippocampal neuronal activity. Nat Neurosci. 2015; 18:1123–1132. [PubMed: 26120964]

Shoop WL, Mrozik H, Fisher MH. Structure and activity of avermectins and milbemycins in animal health. Vet Parasitol. 1995; 59:139–156. [PubMed: 7483237]

Smith DM, Mizumori SJ. Learning-related development of context-specific neuronal responses to places and events: the hippocampal role in context processing. J Neurosci. 2006; 26:3154–3163. [PubMed: 16554466]

Sternson SM, Roth BL. Chemogenetic tools to interrogate brain functions. Annu Rev Neurosci. 2014; 37:387–407. [PubMed: 25002280]

Tanila H, Shapiro ML, Eichenbaum H. Discordance of spatial representation in ensembles of hippocampal place cells. Hippocampus. 1997; 7:613–623. [PubMed: 9443058]

Trichas G, Begbie J, Srinivas S. Use of the viral 2A peptide for bicistronic expression in transgenic mice. BMC Biol. 2008; 6:40. [PubMed: 18793381]

Van Cauter T, Poucet B, Save E. Unstable CA1 place cell representation in rats with entorhinal cortex lesions. Eur J Neurosci. 2008; 27:1933–1946. [PubMed: 18412614]

Van Cauter T, Camon J, Alvernhe A, Elduayen C, Sargolini F, Save E. Distinct roles of medial and lateral entorhinal cortex in spatial cognition. Cereb Cortex. 2013; 23:451–459. [PubMed: 22357665]

Wilson IA, Ikonen S, McMahan RW, Gallagher M, Eichenbaum H, Tanila H. Place cell rigidity correlates with impaired spatial learning in aged rats. Neurobiol Aging. 2003; 24:297–305. [PubMed: 12498963]

Wolstenholme AJ. Recent progress in understanding the interaction between avermectins and ligand-gated ion channels: putting the pests to sleep. Invert Neurosci. 2010; 10:5–10. [PubMed: 20953673]

Yasuda M, Mayford MR. CaMKII activation in the entorhinal cortex disrupts previously encoded spatial memory. Neuron. 2006; 50:309–318. [PubMed: 16630840]

Yasuda M, Johnson-Venkatesh EM, Zhang H, Parent JM, Sutton MA, Umemori H. Multiple forms of activity-dependent competition refine hippocampal circuits in vivo. Neuron. 2011; 70:1128–1142. [PubMed: 21689599]

Yetman MJ, Lillehaug S, Bjaalie JG, Leergaard TB, Jankowsky JL. Transgene expression in the Nop-tTA driver line is not inherently restricted to the entorhinal cortex. Brain Struct Funct. 2016; 221:2231–2249. [PubMed: 25869275]

Ziv Y, Burns LD, Cocker ED, Hamel EO, Ghosh KK, Kitch LJ, El Gamal A, Schnitzer MJ. Long-term dynamics of CA1 hippocampal place codes. Nat Neurosci. 2013; 16:264–266. [PubMed: 23396101]

Highlights

- Transgenic model for spatiotemporal control of neuronal silencing via systemic ligand
- Acute silencing of entorhinal cortex causes global disruption of CA1 spatial tuning
- Concomitant with CA1 remapping, entorhinal silencing degrades spatial recall
- Both place field stability and spatial memory require the same ongoing cortical input

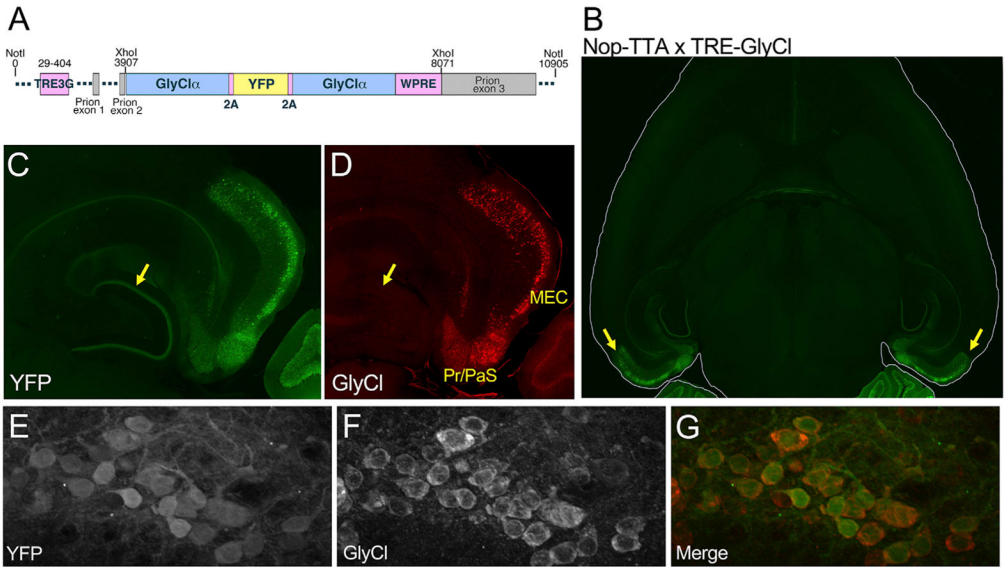

Figure 1. The GlyCl Transgene Vector and Its Expression in the Nop-tTA Model

(A) Viral T2a peptides separate a YFP tag from flanking copies of the modified glycine receptor α subunit, all under control of the tet-responsive TRE3G promoter. The stability of mature processed mRNA was enhanced by incorporation of the first intron from the mouse prion protein gene at the 5′ end and by the WPRE at the 3′ end of the transcript.

(B) Two zones of intense YFP fluorescence are apparent in horizontal brain sections from a Nop-GlyCl mouse: the entorhinal area (shown here) and the cerebellum (shown in Figure S1).

(C) Strong YFP expression is seen in the superficial layers of entorhinal cortex, the neighboring pre- and para-subiculum, and the terminal field of the perforant path in the molecular layer of the dentate gyrus (arrow).

(D) Immunostaining for GlyCl in the section from (C) demonstrates that GlyCl expression is found within the soma of entorhinal and subicular neurons, but is absent from the perforant path (arrow).

(E–G) High-magnification images within the entorhinal cortex show the correspondence between YFP expression (E) and GlyCl immunostaining (F) in a merged image (G) from Nop-GlyCl tissue.

See also Figures S1 and S2 and Table S1.

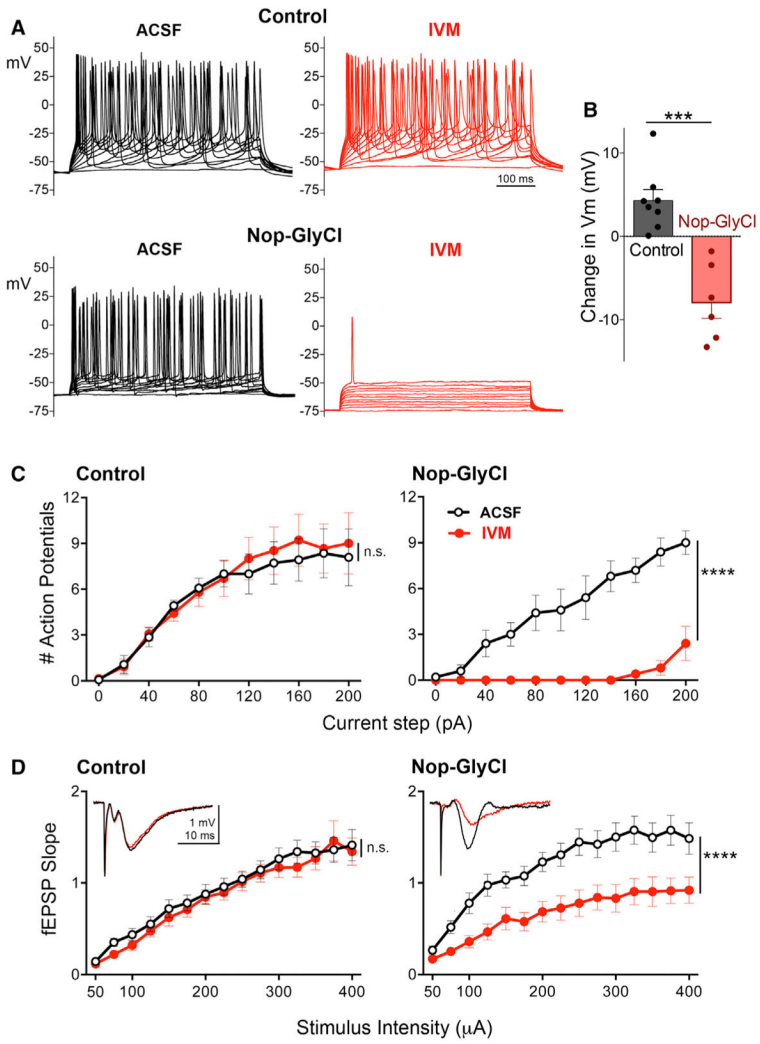

Figure 2. Neuronal Silencing with Ivermectin in Acute Brain Slice Preparations

(A) Example voltage traces from whole-cell recordings in control (top row) and Nop-GlyCl mice (bottom row). GlyCl-expressing neurons initiate action potentials in response to stepped current injection when perfused with ACSF (black) but fail to respond in the presence of 100 nM IVM (red).

(B) Application of IVM hyperpolarized the resting membrane potential of GlyCl-expressing neurons.

(C) In the presence of 100 nM IVM, GlyCl expressing neurons fail to elicit action potentials except at supra-threshold current intensities. Control, n = 7 cells from four animals; Nop-GlyCl, n = 5 cells from five animals.

(D) The excitatory post-synaptic response evoked by perforant path stimulation is reduced by IVM application in Nop-GlyCl brain slices. Insets show representative traces recorded at a stimulation intensity of 200 μA in the presence (red) or absence (black) of IVM. Control, n = 15 slices from six animals; Nop-GlyCl, n = 11 slices from six animals.

See also Table S2.

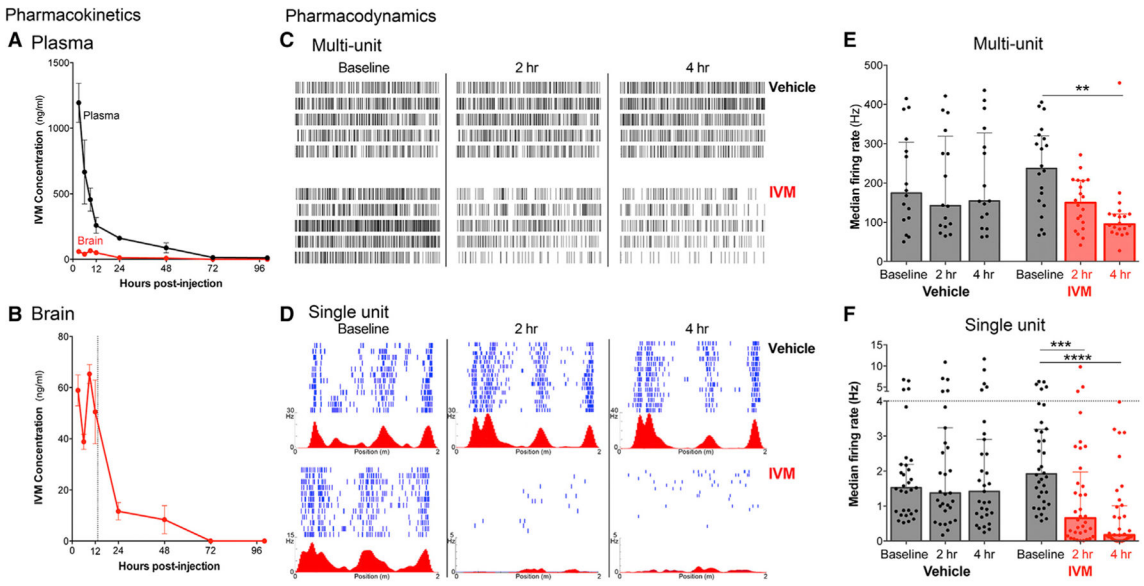

Figure 3. In Vivo Pharmacokinetics and Pharmacodynamics of Ivermectin Silencing

(A and B) Liquid chromatography-tandem mass spectrometry (LC-MS/MS) was used to measure free drug concentration in plasma (A) and brain (A and B) from wild-type mice collected 3 hr to 4 days after a single IVM injection. n = 4 mice per time point (two M, two F). Dotted line indicates $T_{1/2}$ = 13.3 hr.

(C) The pharmacodynamics of IVM at the GlyCl channel was assessed by multi-tetrode recording during open field exploration in CaMKIIα-GlyCl animals. Raster plots show five simultaneous multi-unit recordings (1 trace per tetrode, 2 s of data) taken before, 2 hr, and 4 hr after injection of vehicle (upper row) or IVM (lower row).

(D) Each row of the raster plots shows the action potentials fired by one neuron during sequential laps on the linear track (blue) and average firing rate versus position (red) recorded before, 2 hr, and 4 hr after injection of vehicle (upper row) or IVM (lower row) in CaMKIIα-GlyCl mice. See also Figure S3.

(E and F) Both single- and multi-unit activity in open field remained stable for 4 hr after vehicle injection, but both were significantly reduced by 4 hr after IVM. Data recorded after IVM injection are shown in red. Graphs show median ± interquartile range, each point represents the firing rate at one tetrode (E), or of a single putative pyramidal neuron (F). n = 3 mice.

See also Figure S3 and Table S2.

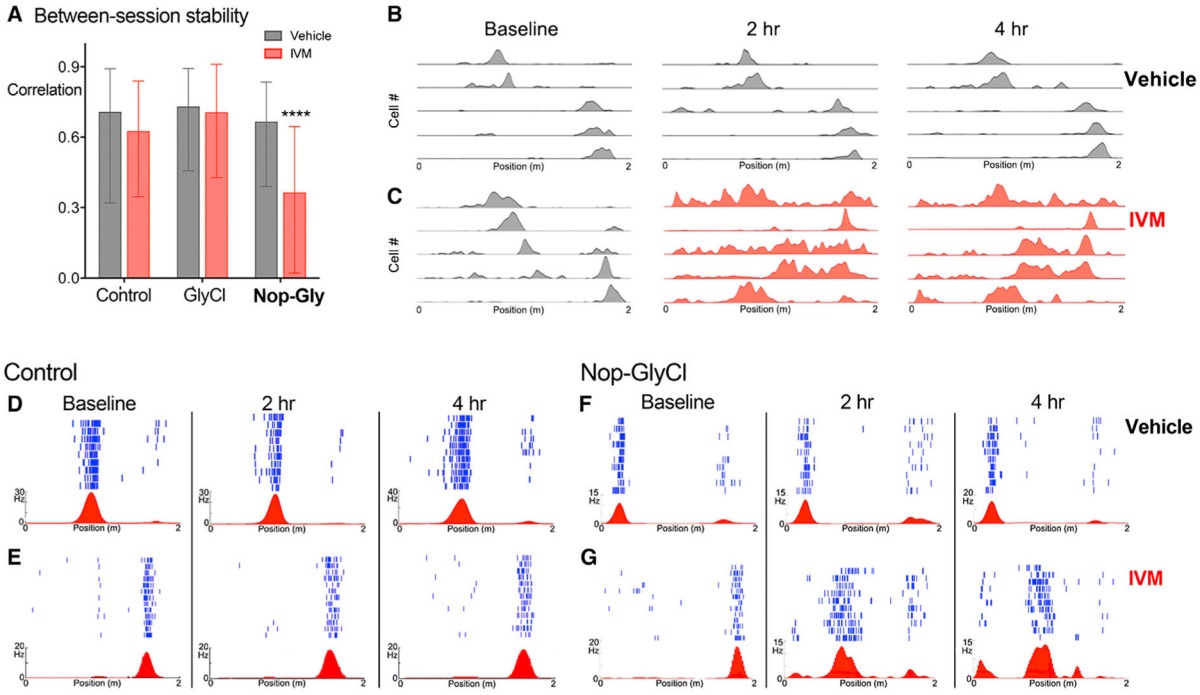

Figure 4. IVM Silencing Causes Place Field Instability in Nop-GlyCl Mice

(A) Between-session stability was measured by the correlation of rate curves computed at baseline with those attained 2 and 4 hr after vehicle (gray) or IVM (red). IVM significantly decreased between-session correlation only for Nop-GlyCl mice. Graph shows median ± interquartile range. n = 4 mice/genotype.

(B and C) Example rate maps from five cells simultaneously recorded in a Nop-GlyCl mouse at baseline each day and again 2 hr and 4 hr after injection of vehicle (B) or IVM (C).

(D–G) Examples of raw data from individual neurons of control (D and E) and Nop-GlyCl mice (F and G) during baseline recording and at 2 hr and 4 hr after injection of vehicle (D and F) or IVM (E and G). Lap-by-lap raster plot of single neuron firing is shown in blue; average firing rate versus linear track position is shown in red.

See also Figures S4 and S5 and Table S2.

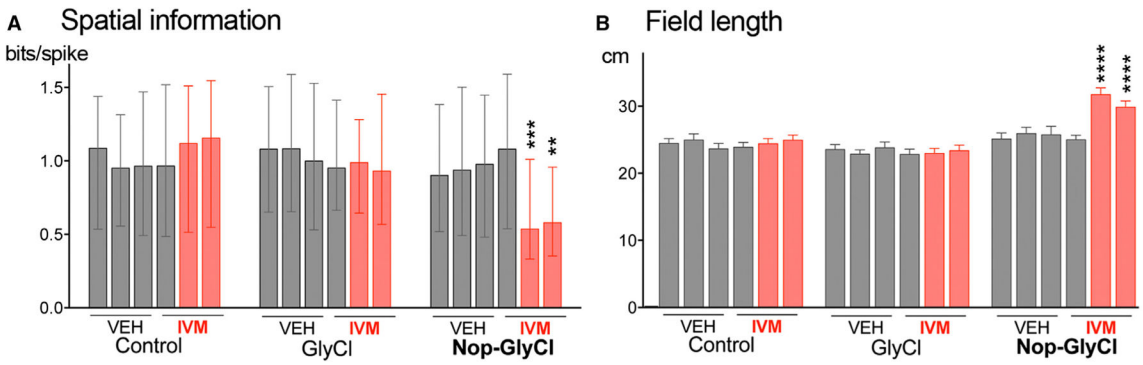

Figure 5. Decreased Specificity of Spatial Tuning following Entorhinal Silencing in Nop-GlyCl Mice

(A) Spatial information was calculated for active cells during each session and remained stable for all genotypes following vehicle injection, but was significantly reduced by IVM in the Nop-GlyCl mice. Data obtained after IVM injection are shown in red. Graph shows median ± interquartile range.

(B) Field length was stable across all sessions in control and GlyCl mice, but increased significantly after IVM administration in Nop-GlyCl animals. Graph shows mean ± SEM. n = 4 mice/genotype.

See also Figure S6 and Tables S2, S3, and S4.

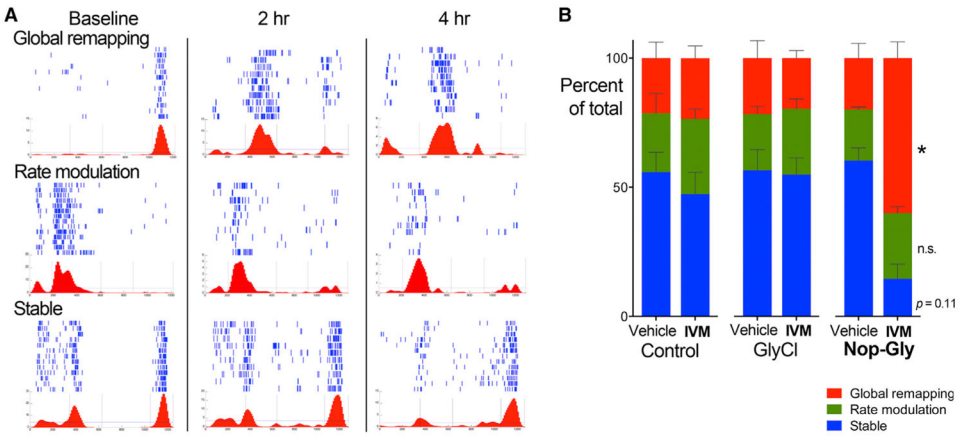

Figure 6. Neuronal Silencing in Nop-GlyCl Mice Induces Global Remapping of CA1 Place Fields

(A) Example cells that underwent global remapping, rate modulation, or remained stable are shown as lap-by-lap spike rasters in blue and average firing rate versus linear position in red. (B) Firing rate curves at baseline were compared with those obtained for the same cell 2 hr and 4 hr after vehicle or IVM injection. The fraction of place fields that underwent global remapping (red), rate modulation (green), or remained stable (blue) was unchanged between vehicle and IVM for control and GlyCl mice, but was significantly shifted toward increased global remapping at the expense of stable fields in Nop-GlyCl mice after IVM injection. n = 4 mice/genotype.

See also Table S2.

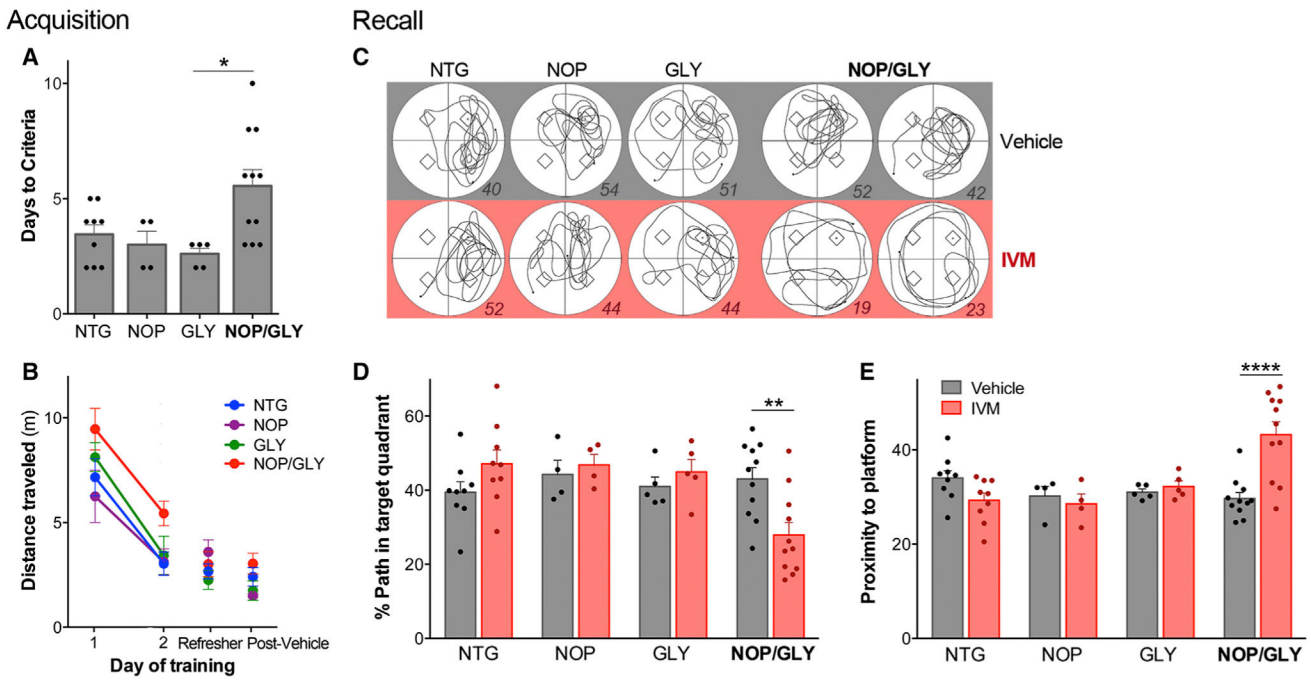

Figure 7. Neuronal Silencing in Nop-GlyCl Mice Impairs Spatial Recall in the Morris Water Maze

(A) A train-to-criteria version of the Morris water maze was used to bring all animals to the same level of performance prior to testing long-term memory. Nop-GlyCl mice took more days of training to master the task than GlyCl single transgenic animals, but ultimately reached the same performance outcomes.

(B) Nop-GlyCl mice traveled longer distances to find the hidden platform during the first two days of training, however, once they reached criteria performance they located the platform with the same efficiency as other genotypes during refresher training.

(C) Track plots show example swim paths taken by each genotype during vehicle (gray) and IVM (red) probe tests. Numbers in italic indicate the % of path spent in the target quadrant for that trial.

(D) Percent of swim path spent in the target quadrant during long-term memory probe tests following vehicle (gray) or IVM (red). Nop-GlyCl was the only genotype for which quadrant occupancy decreased upon IVM administration.

(E) Nop-GlyCl mice swam significantly farther from the trained location after entorhinal silencing than they had following vehicle treatment the previous day. n = 4–11 mice/genotype.

See also Figure S7, Table S2, and Movie S1.